Nuclear Inst. and Methods in Physics Research, A 1048 (2023) 167898

Contents lists available at ScienceDirect

Nuclear Inst. and Methods in Physics Research, A

journal homepage: www.elsevier.com/locate/nima

Characterization and alignment of a resonant cavity beam position monitor for the Compact LInear Collider (CLIC) project at CERN

Silvia Zorzetti [a,b,*], Manfred Wendt [a], Hélène Mainaud-Durand [a]

[a] CERN, Geneva, Switzerland
[b] Fermi National Accelerator Laboratory, Batavia, IL, USA

ARTICLE INFO

Keywords:
Accelerator technology
BPM
LHC
FCC
RF

ABSTRACT

Beam diagnostic devices are essential tools to sense the properties of the beam in particle accelerators. Beam Position Monitors (BPMs) are used to detect the transverse beam spatial coordinates. A large number of high-resolution resonant cavity BPMs, operating at 14 GHz, are proposed to monitor the orbit of the two main beam linacs of the CLIC project. This paper discusses innovative calibration techniques on a dedicated test bench in the frame of the PACMAN project. The particular location of the electromagnetic center of the resonant cavity BPM is detected utilizing a stretched-wire measurement approach. Measurements, RF characterization and final fiducialization of the BPM electrical offset are treated with details. Initial studies through EM simulations of the cavity BPM are covered. The presented experimental results prove the feasibility of the alignment methodology with nanometric resolution.

1. Introduction

The Compact LInear Collider (CLIC) project at CERN is an international study for a future high-energy and high-luminosity particle collider, proposing to collide electrons and positrons with a center-of-mass energy up to 3 TeV [1,2]. The concept to accelerate leptons (electrons or positrons) on a linear trajectory to high, multi-TeV, energies removes the problem of the energy loss due to the synchrotron radiation in a ring accelerator.

$$U_{0,electron} = \frac{e^2\gamma^4}{3\epsilon_0\rho} \approx 88.46\frac{E\ [\mathrm{GeV}]^4}{\rho\ [\mathrm{m}]}\ [\mathrm{keV}] \tag{1}$$

Eq. (1) explains the energy loss that an electron (or positron) experiences on a single turn in a ring collider of radius ρ. That energy loss scales with E^4 and needs to be compensated by a longitudinal force, powered by the RF system. Practically, for multi-TeV ring colliders, this would lead to very large values of ρ due to the power limitations of a real-world RF system, thus to ring accelerators with a very large circumference and consequently, large cost, e.g. for the accelerator tunnel, infrastructure etc.

Table 1 lists some of the most important machine and beam parameters of the CLIC project, which foresees a realization with increasing center-or-mass energy in three stages. Beside the center-of-mass energy, the luminosity $\mathscr{L}$, i.e., the number of particle collisions at the interaction point (IP) per unit time, is a crucial performance parameter [3]:

$$\mathscr{L} = \frac{N^2 n_b f}{4\pi\overline{\sigma}_x\overline{\sigma}_x}. \tag{2}$$

The collision frequency f in Eq. (2) is rather low for linear colliders. For CLIC: $f = f_{rep} = 50$ Hz. In ring accelerators $f = f_{rev}$ is the revolution frequency, which is instead in the kHz regime. Moreover, due to the practical limits for the number of particles per bunch n_b, as well as for the number of bunches N, the effective transverse beam size $\overline{\sigma}_x$ at the IP, which includes a variety of beam–beam effects, has to become very small to meet the luminosity goal of $\mathscr{L} = 5.9\times10^{-34}\ \mathrm{cm}^{-2}\ \mathrm{s}^{-1}$. Detailed optimizations favor a flat beam at the IP, which leads to a particular small vertical beam size at the IP of CLIC, down to 1 nm at the final stage, according to the CLIC implementation plan [4,5].

The smallest achievable transverse beam size at the IP is linked to the transverse beam emittance (ϵ), a beam quality parameter defined for each transverse plane as area of position, $x_i(s)$, and angle, $x_i'(s) = dx_i(s)/ds$, of the beam particles i, in the $x - x'$ phase space, with the beam trajectory s as a parameter. While for an ideal linear accelerator $\epsilon(s)$ is constant, a real-world linear accelerator suffers from emittance blow-up along the beam trajectory, which is typically due to misalignments or unwanted non-linear field effects in the quadrupoles and accelerating structures. Fig. 1(a) illustrates the effect of a misaligned Main Beam Quadrupole (MBQ) of the CLIC accelerator, indicating the trajectories of three charged particles having slightly different momenta, i.e., a typical beam having some energy spread. Due to the transverse offset between the beam trajectory and the center of the quadrupole magnet, the particles experience a deflection, which is slightly different as of their different momenta, and will now travel on different trajectories, resulting in a larger beam size, increased by $\Delta\sigma_y$.

* Corresponding author at: Fermi National Accelerator Laboratory, Batavia, IL, USA.
E-mail address: zorzetti@fnal.gov (S. Zorzetti).

https://doi.org/10.1016/j.nima.2022.167898
Received 1 September 2022; Received in revised form 24 November 2022; Accepted 6 December 2022
Available online 10 December 2022

Table 1
CLIC parameters [1,2,5].

Parameter	Symbol	Unit	Stage 1	Stage 2	Stage 3
Center-of-mass energy	$\sqrt{s}$	GeV	380	1500	3000
Repetition frequency	f_{rep}	Hz	50	50	50
Number of bunches per train	n_b		352	312	312
Bunch separation	Δt_{bunch}	ns	0.5	0.5	0.5
Accelerating gradient	G	MV/m	72	72/100	72/100
Total luminosity	$\mathscr{L}$	1×10^{34} cm^{-2} s^{-1}	2.3	3.7	5.9
Luminosity above 99% of $\sqrt{s}$	$\mathscr{L}_{0.01}$	1×10^{34} cm^{-2} s^{-1}	1.3	1.4	2
Total int. lum. per year	$\int \mathscr{L}$	fb^{-1}	276	444	7-9
Main tunnel length		km	11.4	29.0	50.1
Nb. of particles per bunch	N	10^9	5.2	3.7	3.7
Bunch length	σ_z	μm	70	44	44
IP beam size	σ_x/σ_y	nm	149/2.0	~60/1.5	~40/1
Final RMS energy spread	$\Delta p/p$	%	0.35	0.35	0.35
Crossing angle (at IP)		mrad	16.5	20	20

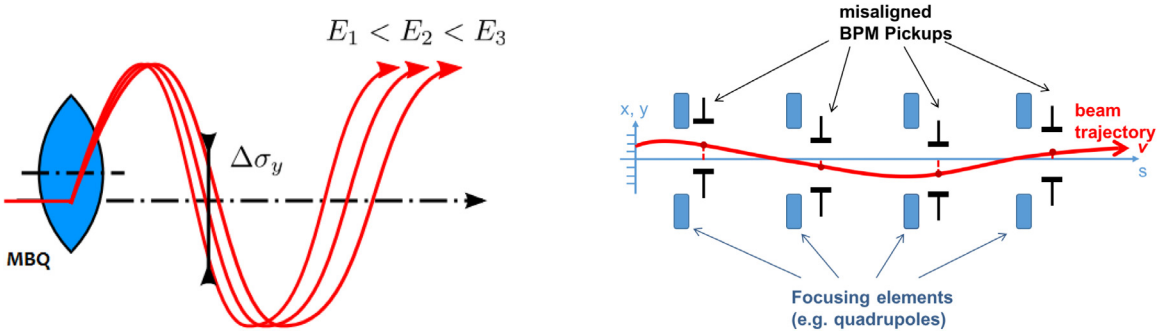

(a) (b)

Fig. 1. MBQ and BPM misalignment effects. (a) MBQ misalignment and particles' energy spread. (b) Typical linac lattice with quadrupole magnets and related BPMs, here misaligned [6].

The same effect happens if the beam is mis-steered through a perfectly aligned quadrupole. Therefore, the beam position monitors (BPMs) are usually located near each quadrupole to monitor and verify that the beam trajectory is exactly aligned to the center of all quadrupole magnets. This requires the BPM pickup itself to be aligned with reference to the center of the quadrupoles. Fig. 1(b) shows an unwanted beam trajectory. The offsets at the quadrupole magnets are due to the misalignment between the BPM pickups and the corresponding quadrupoles, however, the BPMs may still report a perfectly centered beam. These offsets can be corrected through proper alignment and calibration procedures of the BPM devices.

Clearly, the alignment between quadrupole magnets and beam position monitors is mandatory to achieve the luminosity goals of CLIC, and is performed in several iterations [7].

Fiducialization The position of the reference axes of each component is determined w.r.t. external targets. This is used later to reference to the axes, when they are no longer accessible. Metrology tools are used to detect the coordinates and correct the positioning of the components during the assembly and installation procedures.

Electrical-based alignment After rigidly fixing the BPM to the quadrupole magnet, an electrical based alignment procedure determines the offsets and roll-angles between the electrical center of the BPM and the magnetic center of the quadrupole magnet.

Beam-based alignment After the installation and the active pre-alignment of the components, the beam commissioning can take place with a beam-based alignment (BBA) procedure to discover the remaining quadrupole-BPM offset and roll errors by a beam-based measurement procedure.

In frame of the PACMAN (Particle Accelerator Components' Metrology and Alignment to the Nanometer scale) initiative hosted at CERN, the various aspects of pre-alignment, metrology and electromagnetic characterization of the most critical accelerator components have been studied. Using a common stretched wire [8], new solutions to characterize the magnetic axis of a quadrupole [9], the electro-magnetic axis of a high gradient RF cavity [10], and the electrical center of the resonant cavity BPM [11] were proposed, including different methods aiming at the fiducialization of each component within a micrometric accuracy were proposed, based on Frequency Scanning Interferometry (FSI) [12], measurements on a Coordinate Measuring Machine (CMM) [13], and micro-triangulation measurements [14]. This paper summarizes findings and results of a CLIC resonant cavity BPM pickup study and characterization in terms of pre-alignment accuracy of the electrical center utilizing a stretched-wire and RF measurement techniques.

2. Resonant cavity BPMs

While there exist different types and styles of BPM pickups, the resonant cavity BPM is the most promising type to provide sufficient sensitivity to meet the CLIC BPM requirements in terms of resolution and accuracy. The cavity BPM used for CLIC was designed based on the CLIC beam parameters to provide both, high spatial and high temporal resolution, better than 50 nm and 50 ns, respectively [15,16]. The operating frequency of the dipole mode is a design parameter, selected as a compromise between different factors. A higher frequency promises a higher shunt impedance, which results in a higher sensitivity to the beam position, while a sufficient low frequency is required for the mode to be trapped for a given size of the beam pipe ports and

Table 2
Main parameters of the CTF3/CLIC cavity BPM.

Parameter	Symbol	Unit	Value
Monopole resonant frequency	f_{010}	GHz	~11
Dipole resonant frequency	f_{110}	GHz	~15
Maximum loaded Q-factor	Q_L		320
Cavity radius	r	mm	11.24
Waveguides width	a	mm	20
Waveguides height	b	mm	13
Waveguides cut-off frequency	f_{wg}	GHz	~11.5

simplifies the read-out system. Finally, this frequency has to be an integer multiple of the bunch repetition frequency, $1/\Delta t_{\text{bunch}} = 2\,\text{GHz}$ for CLIC (see Table 1). Therefore, the BPM for CLIC is designed to operate at 14 GHz, while, for the prototype the dipole mode eigenfrequency is modified to 15 GHz to comply with the 3 GHz bunched beam structure at the CLIC Test Facility (CTF3) [17]. The CTF3 BPM is shown in Fig. 2(a), RF parameters and geometry are summarized in Table 2, which refers to the diagram in Fig. 2(b).

2.1. Principle of operation

In a passive cylindrical resonant cavity, so-called "pillbox" resonator, the transverse electric (TE) and transverse magnetic (TM) modes are excited as a bunched beam passes through, utilizing the attached beam-ports on either face. If the cavity cylinder holds the geometric relationship of $length < 2 \times radius$, the excited modes are only TM, with eigen-frequencies:

$$f_{nmp} = \frac{1}{2\pi\sqrt{\mu_0\epsilon_0}}\sqrt{\left(\frac{j_{nm}}{r}\right)^2 + \left(\frac{p\pi}{l}\right)^2}, \tag{3}$$

where r is the radius, l is the length of the cavity, and j_{mn} are the roots of the Bessel functions of 1st kind. The TM010 (monopole mode) and the TM110 (dipole mode) are the first two modes excited in this cavity. Those modes follow the boundary conditions described by the zero order and the first order 1st kind Bessel Function ($J_n(x)$, in Fig. 2(d)). With the monopole mode being excited, the maximum of the electric field falls in the center of the cavity, on the z symmetry axis, ($max[J_0(x)] = J_0(0)$, see Fig. 2(d) and dark-blue trace in Fig. 2(c)), while the electric field generated by the dipole mode is zero in the center of the cavity ($J_n(j_{nm}) = 0$, in Fig. 2(d)), observing a change of polarity (light-blue trace in Fig. 2(c)). To operate as beam position monitor, the bunched-beam excited TM110 dipole mode is used, providing a difference (Δ) signal, which depends on the transverse beam position (x), but also on the beam intensity (i_{beam}), the approximation $\Delta \propto x \times i_{beam}$ is valid in the proximity of the electrical center. A beam intensity independent beam position measurement requires normalization of the Δ-signal w.r.t. beam intensity signal, however, this is not needed for the stretched-wire analysis.

Four rectangular waveguides are added to the resonant cavity BPMs, their lowest cut-off frequency depends on the wide dimension a of the rectangular cross-section:

$$f_{wg} = \frac{1}{2a\sqrt{\mu_0\epsilon_0}}, \tag{4}$$

where μ_0 and ϵ_0 are the vacuum permeability and permittivity, respectively. Selecting the cut-off frequency of the waveguides in-between the monopole and the dipole eigen-frequencies of the pill-box cavity ($f_{010} < f_{wg} < f_{110}$) allows a very efficient discrimination of the dipole mode signal with respect to the monopole mode signal, which is always excited by the bunched beam. Moreover, the slot-coupled waveguides define the two polarization axes of the TM110 mode, usually oriented to the horizontal (x) and vertical (y) plane. Modes' selectivity and orientation are displayed in Fig. 3. With the added waveguides, the cavity BPM behaves as common-mode free differential detector (CM-free cavity BPM), providing two separate TM110 Δ-signals being proportional to the horizontal and vertical beam position, thus enable a beam position measurement in 2D Cartesian coordinates (horizontal and vertical).

2.2. Signal processing

A simple beam position measurements system is composed by sensing beam pickups and read-out electronics. A generic block diagram is shown in Fig. 4, depicting the signal treatment chain, from the detection to the analogue and digital signal processing [6]. Commonly used beam pickups are based either on broadband electrostatic, electromagnetic, or on resonant operational principles [18]. In case of broadband BPM pickups, pairs of symmetrically arranged electrodes couple to the electromagnetic field of the beam and output a voltage signal $V_{pickup}(\omega)$, which is proportional to the beam current $I_{beam}(\omega)$, and to the beam displacement, i.e., transverse beam position (x, y). This is expressed in Eq. (5), where $s(x, y, \omega)$ is a sensitivity term associated to the beam coupling method, and $Z_{PU}(\omega)$ is the transfer impedance given by the pickup geometry and the materials being used.

$$V_{pickup}(\omega) = s(x, y, \omega) Z_{PU}(\omega) I_{beam}(\omega) \tag{5}$$

Some of the eigenmodes of a single-cell, cylindrical resonator used as cavity BPM are excited by the bunched beam, thus, the cavity BPM can be viewed as a band-pass filter. Beside the eigenfrequency, given by the size of the resonator, each mode can be characterized by the shunt impedance over the unloaded quality factor (R/Q_0). The unloaded Q-factor is determined by the losses in the cavity walls:

$$Q_0 = \frac{\omega U}{P}, \tag{6}$$

where U is the energy stored, P is the power dissipated in the resonator, and ω is the resonant frequency of the cavity.

The shunt impedance should be as high as possible to achieve high sensitivity. It is calculated as:

$$R = \frac{V^2}{P}, \tag{7}$$

where $V = \int_{-l/2}^{+l/2} E_z dz$ is the gap voltage across the cavity, l is the length of the cavity.

The ratio between the shunt impedance and the quality factor only depends on geometry and not on losses in the materials. Eq. (8) defines the normalized shunt impedance for the TM110 mode as in Ref. [19], at an offset $r_0 = x_0$ or y_0, depending on the TM110 mode polarization, horizontal or vertical, respectively.

$$\frac{R}{Q_0} = \frac{V^2}{\omega U} = \left[\frac{R_s}{Q_0}\right]_{r_0} \frac{r^2}{r_0^2}, \tag{8}$$

Compared to the broadband BPM pickups, like stripline or button BPMs, the shunt impedance R of a cavity BPM for the TM110 dipole mode resonance typically is several orders of magnitude higher (a few Ω/mm vs. some kΩ/ mm), which results in higher sensitivity [15].

The voltage induced into a load impedance Z_{load} (typically, $Z_{\text{load}} = R_{\text{load}} = 50\ \Omega$), coupled to the cavity BPM with a coupling given by $1/Q_{\text{ext}} = 1/Q_L - 1/Q_0$, by a gaussian beam bunch of length σ_z and charge q, passing the BPM resonator at a relativistic velocity $v \approx c$ follows then as:

$$v_r(t) = V_{\text{out}} e^{-\frac{t}{2\tau}} \sin(\omega t), \tag{9}$$

$$V_{\text{out}} = \frac{\omega}{2} q \frac{r}{r_0} \sqrt{\frac{Z_{\text{load}}}{Q_{\text{ext}}} \left[\frac{R}{Q}\right]_{r_0}} \exp\left(-\frac{\omega\sigma_z^2}{2c^2}\right), \tag{10}$$

with r/r_0 being the horizontal $r = x$ or vertical $r = y$ beam displacement w.r.t. an offset as defined for $[R/Q_0]_{r_0}$, parallel to the z-axis. It follows from Eqs. (9) and (10) that the voltage on the load depends linearly on

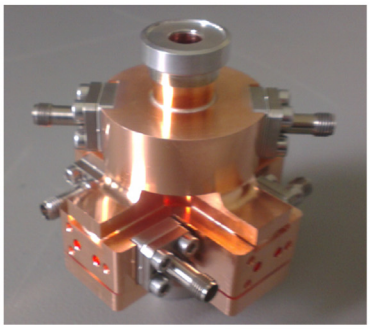

(a)

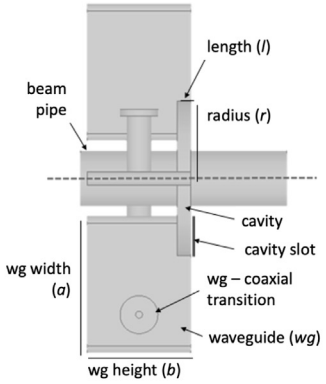

(b)

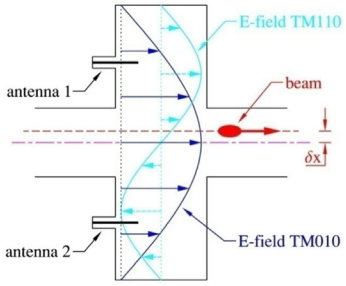

(c)

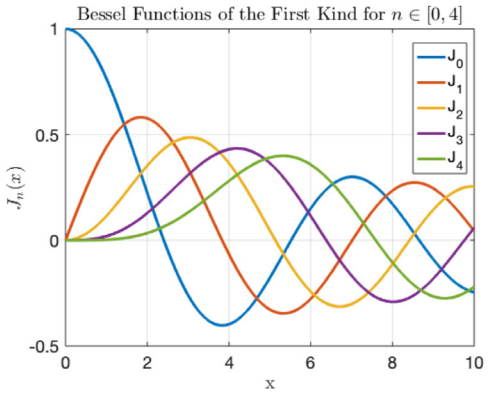

(d)

Fig. 2. (a) Picture of the cavity BPM prototype for the CTF3 facility, made of copper. (b) Parts and dimensions of the CLIC cavity BPM. (c) Monopole and dipole modes trends in a pillbox cavity. (d) The TM010 and TM011 follow the trends of the $J_0(x)$ and $J_1(x)$, respectively.

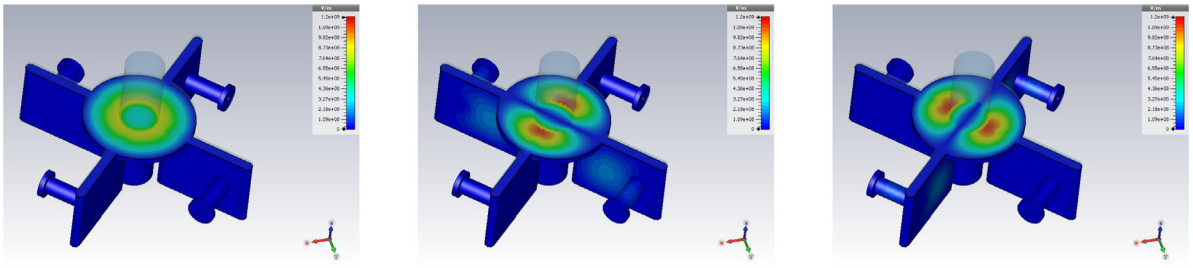

(a) (b) (c)

Fig. 3. Microwave eigenmode simulations of the resonant cavity BPM used for CLIC. The magnitude values of the electric field are projected on the central cross-section of the pillbox resonator. (a) Monopole mode, TM010. There is no coupling between the cavity and the waveguides if the monopole mode is excited. (b) Dipole mode TM110 (horizontal polarization). (c) Dipole mode TM110 (vertical polarization). b–c In presence of a dipole mode excitation the signal is detected and passes through the waveguides to the coaxial ports. The two different polarizations of the dipole mode are aligned to the orthogonal set of external waveguides.

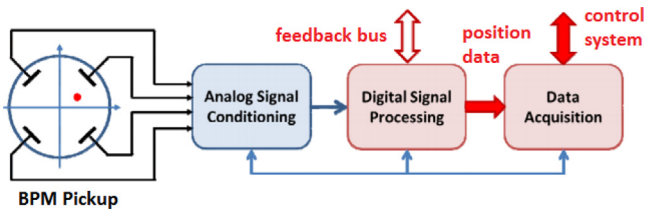

Fig. 4. Generic BPM system block diagram [6].

the beam displacement r: $v_r(t) \propto r\, e^{-\frac{t}{2\tau}} \sin(\omega t)$. This approximation is valid over a range of approximately two-thirds of the beam pipe [19]. It is also noted that the maximum power is transferred in critical coupling: $Q_L = Q_{\text{ext}} = Q_0/2$.

In a similar way, we can compute the voltage induced by a particle beam passing through the cavity BPM with pitch and yaw angles α and θ:

$$V_\alpha(t) \propto -\alpha e^{-t/2\tau} \cos(\omega t), \tag{11}$$

$$V_\theta(t) \propto \theta e^{-t/2\tau} \cos(\omega t), \tag{12}$$

limits apply to $\alpha \ll 1, \theta \ll 1$. Further analysis and detailed calculation can be found in Refs. [19,20]. Using a simplified notation, the cavity's output signal $v(t)$ is proportional to three components:

$$v(t) \propto q e^{-t/2\tau} e^{-i\omega t} (S_x x + S_\alpha \alpha e^{i\pi/2} + S_\theta \theta e^{-i\pi/2}) \tag{13}$$

where S_x, S_α and S_θ are the linear beam displacement (beam position), the beam angle, and the bunch tilt sensitivities, respectively, which can be determined by appropriate calibration procedures [21]. The analysis the TM110 sinusoidal signal in the complex plane as in-phase (I) and quadrature-phase (Q) components enables the detection of both the linear (beam displacement) and the angular (bunch tilt) information: $I = A\cos(\phi)$ and $Q = A\sin(\phi)$, where A and ϕ are the amplitude and the phase of the acquired signal, respectively.

3. Perturbing wire analysis

Any BPM pickup utilizes a symmetric geometrical structure to detect and measure the transverse beam position. In the case of the cavity BPM it is the symmetry of a cylinder and the related TM110 dipole eigen-mode. To locate the dipole mode electric symmetry axis of an imperfect cylindrical cavity BPM we use a stretched wire as a passive probe. With a conductive wire stretched through the cavity, monopole-like, dipole-like and higher-order modes (HOMs) are still present. The electric field on the wire surface is null because the tangential electric field component on the wire surface is zero ($\Phi = 0 \rightarrow E_t = 0$, assuming a high conductivity of the wire). Fig. 5 shows the magnitude of the normalized electric fields for one polarization of the TM110 dipole mode, including the perturbation introduced by the stretched wire. As the wire is moved along the horizontal axis, the symmetry of the TM110 mode is broken, and the electric field is forced to zero at the location of the wire. For dipole modes, the electric symmetry is restored if the wire is placed in the central location. The electrical center is indeed the location of minimum perturbation in the cavity BPM.

3.1. Frequency shift analysis based on Slater's theorem

Any perturbation of a resonant mode will cause a shift of the eigen-frequency, that can be detected as a frequency-shift. The Slater's theorem describes the interaction between the magnetic permeability (μ_r) and the electric permittivity (ϵ_r) of a dielectric or conductive object positioned in an empty resonant cavity [22]. The frequency shift of the eigen-frequency caused by this effect is given by:

$$\frac{\Delta\omega}{\omega_0} = \frac{\omega - \omega_0}{\omega_0} = \frac{\int_{\Delta_V} (\mu_0\mu_r|H|^2 - \epsilon_0\epsilon_r|E|^2) dV}{\int_V (\mu_0|H|^2 + \epsilon_0|E|^2) dV} \tag{14}$$

with H and E being the magnetic and electric fields of the eigenmode, which depend on the position of the object, and ω_0 the unperturbed eigen-frequency. The nominator of the Eq. (14) is an integral over the volume of the resonant cavity subtracted by the volume of the perturbation (ΔV), which results in the energy stored in the perturbed system. The denominator of Eq. (14) is instead the energy stored in the unperturbed resonator (U_0), calculated over the entire cavity volume (V). If a thin cylinder, in our case a metallic wire, is positioned along the longitudinal direction of an empty cavity, it perturbs the resonant modes according to Slater's theorem. Both, the magnetic and the electric fields are influenced by this object, however, if it is made of paramagnetic material ($\mu_r \approx 1$), the perturbation is prevalent on the electric field [23]:

$$\frac{\Delta\omega}{\omega_0} = \frac{\epsilon_0 V_p}{2U_0} \frac{\epsilon_0 - 1}{\epsilon_0} E_0^2, \tag{15}$$

where V_p is the volume of the perturbing object. The frequency perturbation is proportional to the electric field strength. This allows us to qualitatively reconstruct the E-field pattern and to precisely locate the electrical symmetry axis in the BPM cavity, and in a following step to determine the misalignment of the BPM w.r.t. the magnetic axis of a CLIC MBQ quadrupole.

4. Microwave characterization of the resonant cavity BPM

As part of the PACMAN project, we studied and verified the nanometric resolution of the cavity BPM using our stretched-wire measurement setup. Furthermore, the CLIC BPM was also studied with beam at the CLIC Test Facility CTF3, and this activity is still continued at the CERN Linear Electron Accelerator for Research (CLEAR) [24]. For the PACMAN project the alignment and calibration procedures were performed on a dedicated, beam independent test bench, utilizing the stretched-wire RF measurement approach, see Fig. 6.

4.1. Stretched wire setup

A single thin metallic wire stretched through a metal tube and excited with an RF stimulus signal generates only transverse electric and magnetic field components (TEM) that propagate along this coaxial transmission-line, for all frequencies below a cut-off frequency given by the cross-section dimensions. The electromagnetic fields of this coaxial wire setup are almost identical to that of a charge particle beam traveling at a relativistic velocity $v \approx c$. If the wire is used as a passive perturbation probe, it couples to the electrical field generated in the BPM resonator by signals fed via the lateral waveguides. Unwanted power dissipation and signal degradation might be induced as well. However, this method substantially simplifies the electrical measurements process, as it avoids RF impedance matching and signal transport lines at higher frequencies. This method is used to locate the electrical center of the CLIC cavity BPM with high accuracy. The metallic wire used for this setup is made of Cu–Be and has a diameter of 100 μm.

4.2. Actuators - Translation stages

The conductive wire is fixed on both ends by support columns mounted on an optical table and stretched through the cavity BPM, which is mounted rigidly on a high-precision 6-axis translation stage (hexapod), sitting on the same optical table, see also Fig. 6. The cavity BPM is moved in sub-micrometer steps along the linear horizontal or vertical axes, and in sub-microradian increments for both corresponding angles, pitch and yaw, while the stretched wire is fixed. Applying

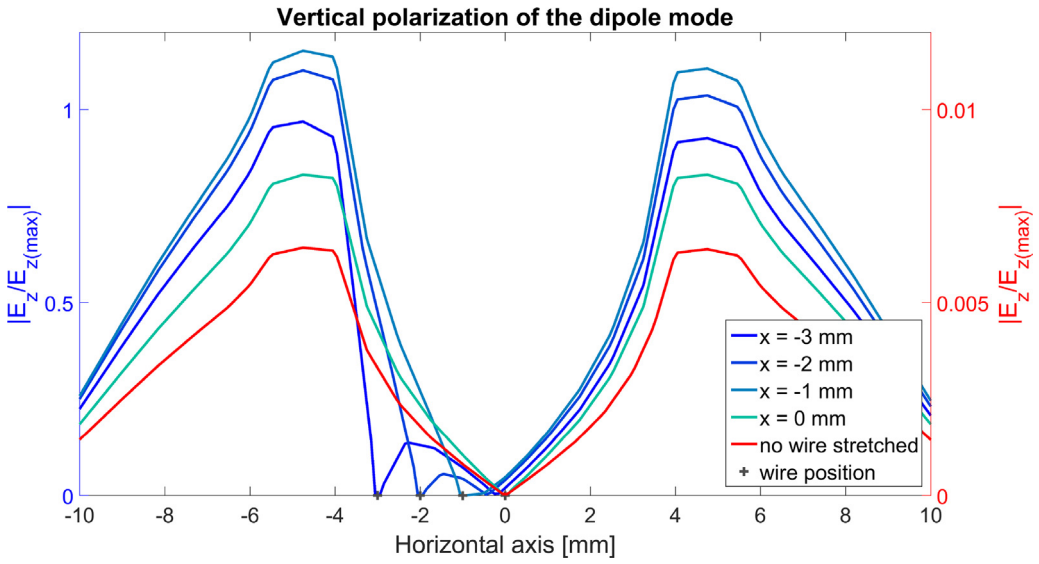

Fig. 5. Normalized electric field. Dipole mode perturbation induced by the wire.

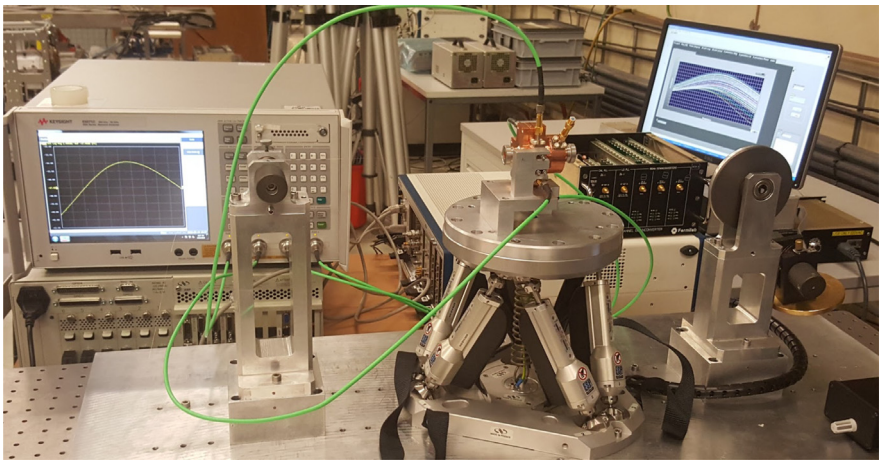

Fig. 6. CLIC beam position monitor test bench.

small displacement steps to the hexapod allows to scan the horizontal and vertical position of the BPM cavity with reference to the wire, after having compensated remaining tilt and rotation errors, which enables to qualitatively reconstruct the modulus of the electric field of the TM110 mode for the two polarizations utilizing S-parameter measurements with a vector network analyzer (VNA) on the four signal ports of the cavity BPM.

4.3. Port coupling measurements

As the dipole-mode field cannot be measured directly, we used the four coaxial signal ports, each located near the end of the corresponding rectangular waveguide that couple through a slot to the cavity resonator, to investigate the field symmetry as we moved the cavity BPM w.r.t. the stretched wire to locate the symmetry axis. A 4-port vector network analyzer (VNA), operated at the dipole mode frequency, was used to measure the scattering parameters or S-parameters at the four ports.

- Analyzing the transmission S-parameters between two *opposite ports*, i.e., the horizontal or the vertical signal ports on the waveguides of the cavity BPM will give the power transmission for a given wire location. If the wire is located in the electrical center, the coupling to the electric field components is minimum, and the power transmission between those opposite ports is maximum. The phase argument however does not return any valuable information, as the power transmission always happens in the same polarization plane.
- Another option is to analyze the transmission coefficients between *adjacent ports*, noting that the cavity construction is optimized for a low cross-talk between the horizontal and vertical plane (~40 dB). In this case, with the wire in the electrical center, the perturbations are minimum, and therefore the power transmission between two *adjacent ports* is reduced to a minimum. Even in this low-coupling situation, the VNA has sufficient dynamic range to precisely identify the minimum of the magnitude of the transmission parameter, moreover the phase argument 'jumps' as the wire crosses the electrical center, which offers a particular high sensitivity and resolution to locate the electrical center.

4.4. Frequency perturbation

We analyzed the frequency shift on the resonant cavity BPMs caused by the wire, as described by Eq. (15). The frequency shift is proportional to the wire displacement, i.e. the perturbation, and therefore it

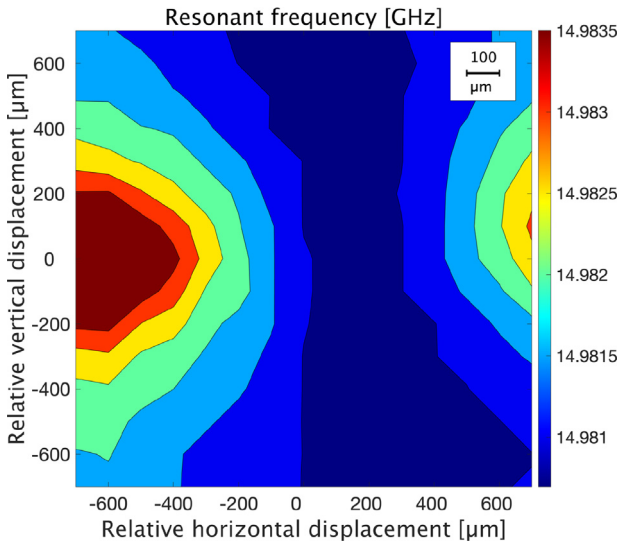

Fig. 7. Frequency perturbation induced by the stretched-wire on the dipole eigen-frequency.

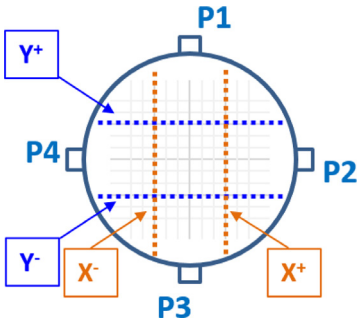

Fig. 8. BPM electrical center location method through wire scan on the linear directions.

is equivalent to the magnitude of the E-field of the dipole mode. While scanning the cavity w.r.t. the wire over a transverse section of the BPM near the center (±700 μm), along horizontal and vertical directions, the reflection coefficients $|Snn|$ on the ports were monitored over a relevant frequency range and stored for each step. Fig. 7 shows the result after analyzing the frequency-shift from the S-parameter data correlated with the wire location.

5. Analysis of the electrical center

Applying the stretched-wire perturbation method discussed above, in an initial attempt we scanned the xy - plane of the cavity BPM around the geometric center over an area of ±1 mm in rather coarse steps of 100 μm. For the analysis of the S-parameters only a single frequency at resonance was used from the VNA data, ports P1 and P3 are the vertical signal ports and P2 and P4 are the horizontal signal ports. Fig. 8 shows the diagram of the input–output microwave ports in the resonant cavity BPM.

Opposite ports: Analyzing the magnitude arguments of the scattering parameters between the opposite ports for each wire location returns patterns which are inverse proportional to the two polarizations of the TM110 dipole electric field, see Fig. 9. Before the actual scan, the roll angle of the cavity BPM was carefully aligned to the horizontal and vertical axes of the hexapod, as seen in the patterns of $|S31|$ (Fig. 9(a)) and $|S24|$ (Fig. 9(b)), which are perfectly orthogonal. This enables the location of the electrical center for each axis, horizontal and vertical. As expected, the phase arguments between opposite ports $\angle S31$ (Fig. 9(c)) and $\angle S24$ (Fig. 9(d)) do not offer additional valuable information.

Adjacent ports: Analyzing the S-parameter transmission coefficient between adjacent signal ports gives a better handle to precisely locate the electrical center of the cavity BPM. Just a single S-parameter, e.g. $S41$ (Fig. 10), reveals the entire xy-symmetry of the resonator, and also more pronounced, the location of the electrical center. This is due to the fact that, with the wire in the electrical center at minimum perturbation, the localization of the minimum magnitude of a transmission coefficient is more precisely compared to a broad maximum as for the opposite port analysis. In the ideal case, it would be a singularity, here the minimum is limited by the finite $x - y$ cross-talk of the two TM110 mode polarizations. Moreover, the phase of the transmission parameter between adjacent ports changes by 180 - degree as the wire location crosses the horizontal or vertical axis, see Fig. 10(b), and gives additional valuable information to precisely locate the electrical center.

5.1. Fine tuning of the electrical center location

Instead of scanning the entire xy - plane of the cavity BPM near the electrical center we prefer a more tailored scan and analysis procedure with focus on one DOF (degree-of-freedom) at the time. In this way, we also minimize the influence of remaining backlash errors of the hexapod. Fig. 8 illustrates the principle, we select two horizontal and two vertical linear scans, always with the orthogonal axis fixed, the steps are indicated as dotted lines in the graphic. For our preferred S-parameter analysis format, $\angle Sij$, those linear scan trajectories are indicated in the general result of $\angle S41$ of Fig. 10(b). For the 2 + 2 linear scans, the horizontal (X^+ and X^-) and vertical offsets (Y^+ and Y^-) are chosen to be approximately symmetric to the electrical center, as indicated by the coarse analysis. In a similar way, we also need to scan the two angular DOF, pitch (v-axis) and yaw (w-axis), again with 2 + 2 angular scans for a set of angular offsets, e.g., W^+ and W^- while performing the v-axis scans.

Fig. 11 shows the results of the linear scans for coarse steps of 100 μm over a range of ±1 mm for the two vertical trajectories (X^+ and X^- in Fig. 11(a)) and for the two horizontal trajectories (Y^+ and Y^- Fig. 11(b)), utilizing $\angle S14$, which is identical to $\angle S41$ because our four signal-port cavity BPM is a reciprocal network ($Sij = Sji, \forall i, j, i \neq j$). It illustrates the 180-degree phase jump as the wire crosses the symmetry axis, demonstrating the high sensitivity of the Sij phase measurement on adjacent ports, and the symmetric behavior of the phase argument for the two measured trajectories. The crossing of X^+ and X^- (Fig. 11(a)) and the crossing of Y^+ and Y^- (Fig. 11(b)) give the electrical center coordinates on the vertical and horizontal axes, respectively.

Fig. 12 shows the same $\angle S14$ trajectories, but now for a narrow range of ± 100 μm near the electrical center, as identified in Fig. 11, and by scanning the hexapod in smaller incremental steps of 10 μm. Now the phase's trend in $\angle S14$ vs. wire location appears as an almost linear transition, allowing to fit the data points by a simple linear interpolation:

$$\begin{cases} x_0 = m_x x + a_x \\ y_0 = m_y y + a_y \end{cases} \tag{16}$$

with m_x and m_y being the gradient (hence the sensitivity) of the straight line fits, and a_x and a_y being some constants due to the phase offsets.

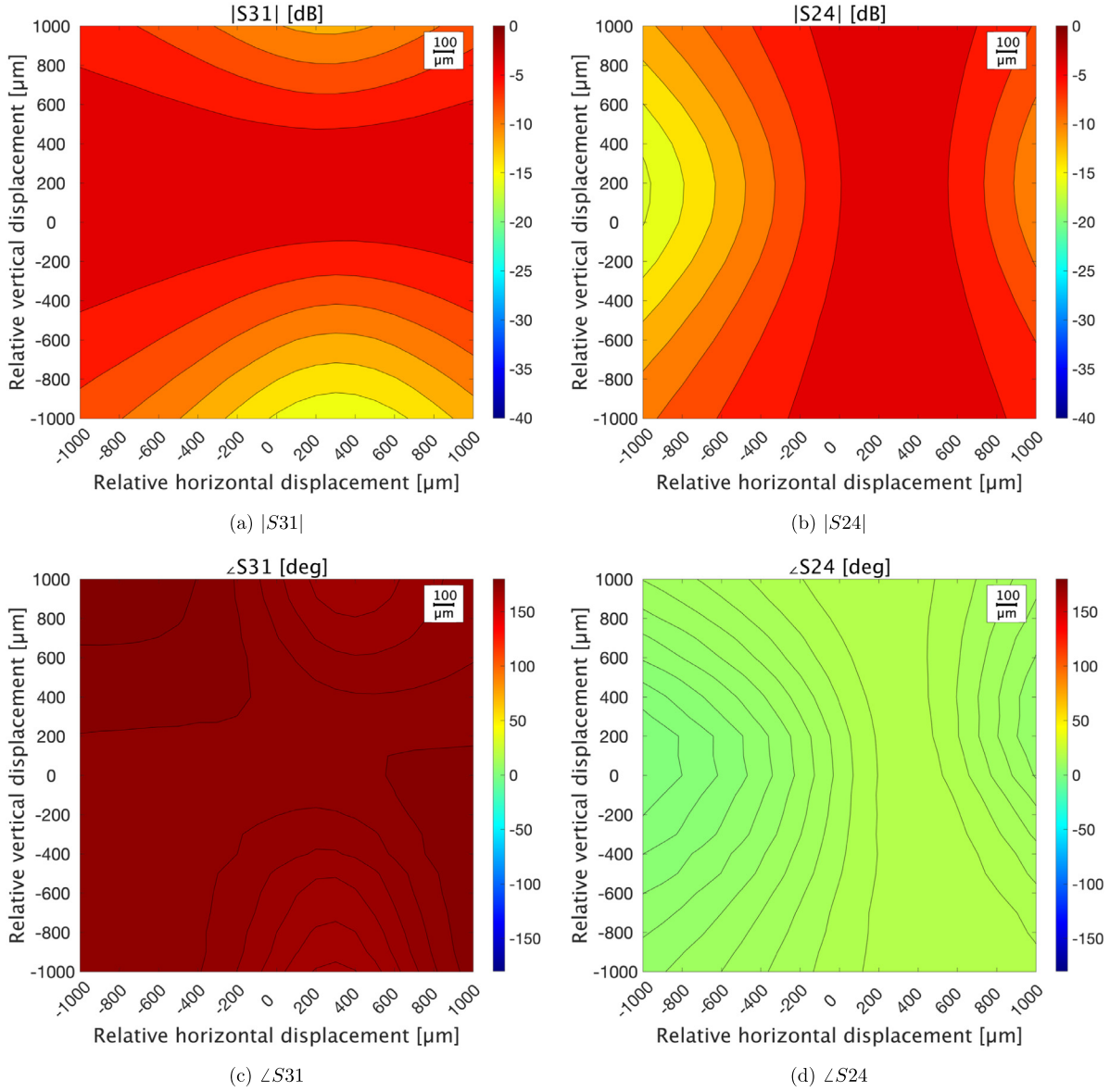

(a) $|S31|$ (b) $|S24|$

(c) $\angle S31$ (d) $\angle S24$

Fig. 9. 2D linear xy - scan of the cavity BPM position w.r.t. the wire. The magnitude and phase arguments of the transmission S-parameters between opposite (horizontal and vertical) signal ports are plotted. The scan step size increment is 100 µm.

5.2. The effect of angular errors

Following the above method of the adjacent port signal analysis, we can collect and analyze four S-parameters, $\angle S14$, $\angle S34$, $\angle S12$ and $\angle S23$ to locate the electrical center from the $2+2$ linear scans. Ideally, all four datasets should report the same value for the electrical center. However, comparing the results of the linear position scans of e.g. $\angle S14$ and $\angle S34$ (see Fig. 13) reveals a small, but clearly identified difference in the location of the electrical center for both axes, horizontal and vertical, in the order of approximately $1/2$ step size (5 µm). This difference can be explained by remaining angular errors, pitch and yaw, such that the symmetry z-axis of the BPM and the wire are not perfectly parallel.

To better understand the effect of the angular errors on the determination of the electrical center from the $\angle Sij$ data, a scan of the cavity BPM around the two angular directions (v and w) should be performed. Due to the kinematics of the hexapod, while performing angular increments, small linear translations are added. In our case, we took advantage from the hexapod internal translation effects, simultaneously acquiring data for the position movements in all directions of interest. We covered all possible combinations for the 4 degrees of freedom (DOF), x, y, v, w movements, therefore detect the electrical center by only scanning the two angular axes, v and w. We followed the same methodology used for the linear axis, with the difference that we now had to scan along fixed angular trajectories, V^- and V^+ for the scan around the horizontal (pitch) angular axis, and W^- and W^+ for the scan on the vertical (yaw) angular axis. Again, the cross point between the two scan results were calculated by a linear regression, as best fit interpolation between the recorded data values.

Fig. 14 shows the results of the angular scans discussed in the previous paragraph. Here, the indicated horizontal and vertical positions are referred to the hexapod's internal position coordinates, which is provided by its close-loop feedback circuit.

The results of the combined angular and linear scans are summarized in Table 3, based on the analysis of the transmission coefficients using ports P1 and P4 for the stimulus signal. The variances between the calculated electrical center coordinates are in the sub-µm and mdeg range. Those residual misalignment errors are comparable with the hexapod accuracy, but also to the geometric asymmetries of the cavity BPM due to manufacturing imperfections, as well as from remaining asymmetries in the signal port coupling.

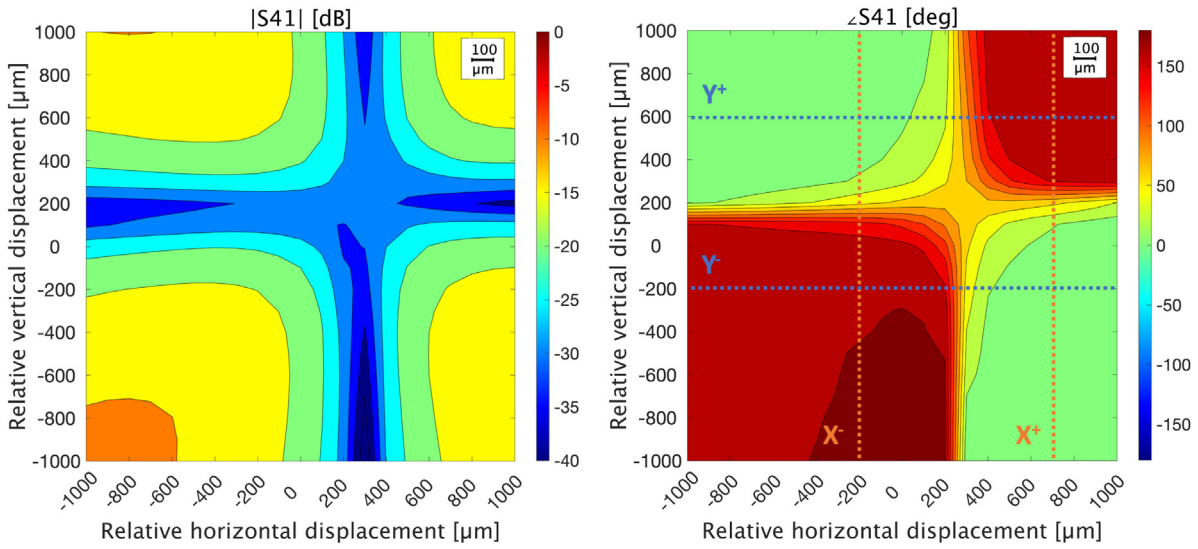

(a) $|S41|$ (b) $\angle S41$

Fig. 10. 2D linear xy - scan of the BPM position cavity w.r.t. the wire. The magnitude and phase arguments of transmission S-parameters are acquired between adjacent ports P4 and P1. The scan step increment is 100 µm.

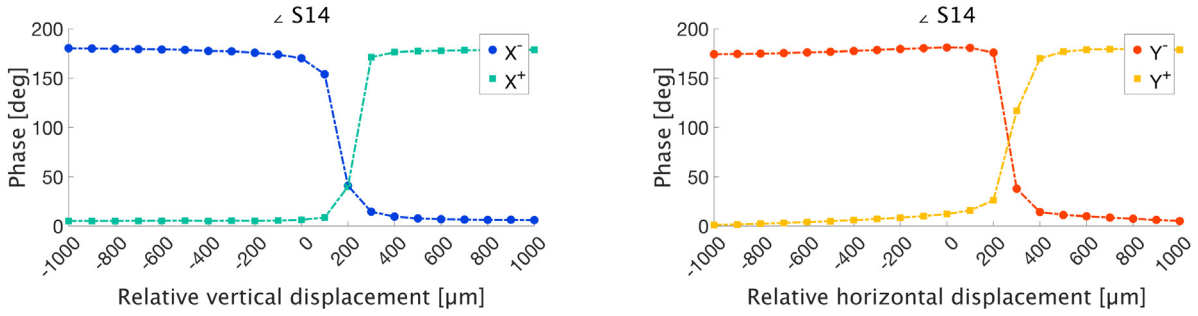

(a) $\angle S14$ vertical scans. (b) $\angle S14$ horizontal scans.

Fig. 11. Phase response of $S14$ for two linear scans in steps of 100 µm.

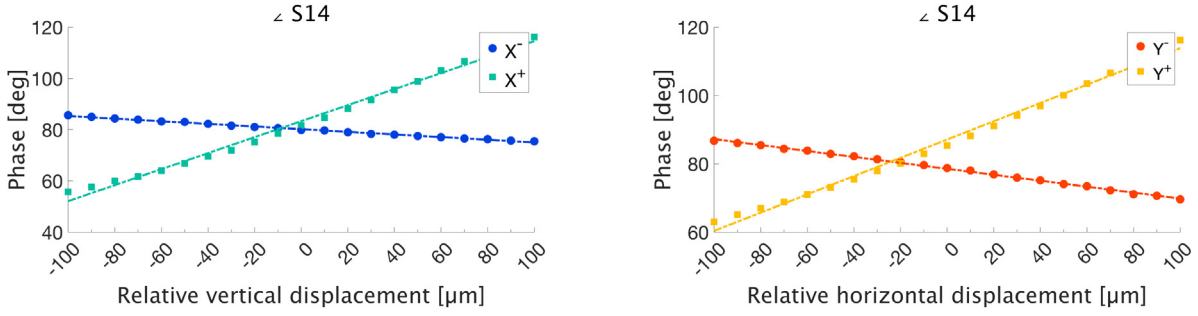

(a) $\angle S14$ vertical scans. (b) $\angle S14$ horizontal scans.

Fig. 12. Phase response of $S14$ for two linear scans in steps of 10 µm.

5.3. Nanometric position resolution of the cavity BPM

The anticipated high resolution potential of the CLIC cavity BPM was outlined in Ref. [17], based on a numerical optimization procedure. With an $R/Q \approx 3\ \Omega/\text{mm}$ and a loaded Q-value of $Q_L \approx 300$ for the TM110 dipole mode, the achievable position resolution for a single bunch at a nominal charge of 1 nC should be around 200 nm. This limitation is mainly given by the leakage of the TM210 quadrupole and the TM010 monopole modes, which are also excited by the bunched beam. In our laboratory setup, analyzing the BPM purely at the TM110 dipole mode frequency the resolution is mainly given by the signal-to-noise ratio of the measurement instrument and the environmental noise, such as temperature and vibrations. With our stretched-wire test bench, we

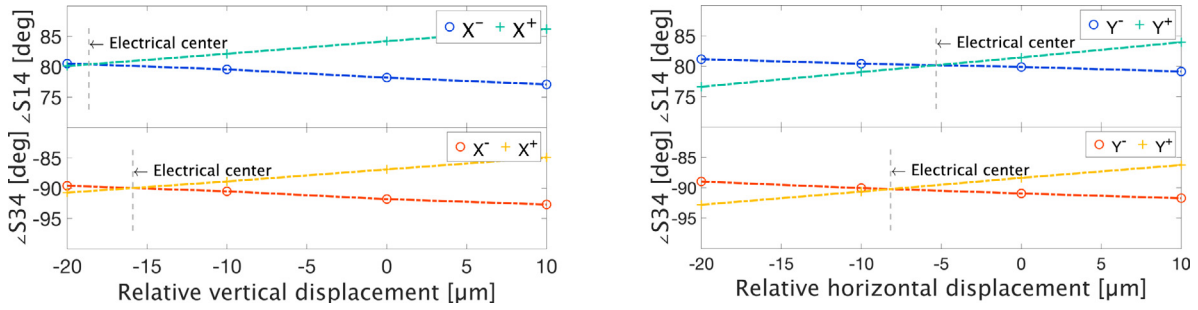

(a) $\angle S14$ and $\angle S34$ vertical scans. (b) $\angle S14$ and $\angle S34$ horizontal scans.

Fig. 13. Relative coordinates of the electrical center from $\angle S14$ and $\angle S34$. The scan step increment is 10 μm.

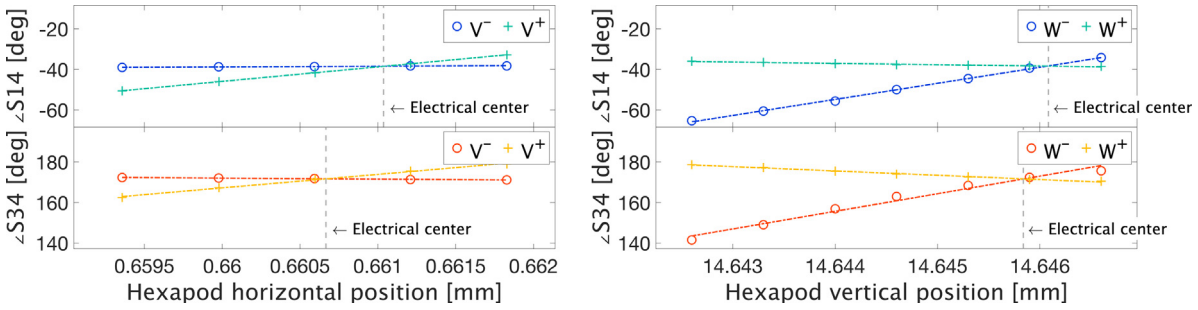

(a) $\angle S21$ and $\angle S41$ horizontal scans. (b) $\angle S21$ and $\angle S41$ vertical scans.

Fig. 14. $\angle S21$ and $\angle S41$ vs. combined angular/linear scans, referenced to the hexapod's internal position coordinates.

Table 3
Electrical center coordinates referred sensed by the hexapod feedback hardware.

Axis	Hexapod position					Average	Variance
coordinate	S21	S41	S14	S34	Unit		
X	0.6613	0.6611	0.6610	0.6607	mm	0.6610 mm	0.26 μm
Y	14.6498	14.6499	14.6488	14.6498	mm	14.6461 mm	0.13 μm
W	0.00409	0.0071	0.0104	0.0267	deg	0.0041 deg	10.13 mdeg
V	−0.8345	−0.8540	−0.8540	−0.8842	deg	−0.8345 deg	20.53 mdeg

demonstrated the high-resolution of the cavity BPM by nanometric wire scans through the cavity. This method is substantially simpler than a bunched beam setup, which often requires the setup of three identical cavity BPM in a ballistic optics configuration to eliminate the beam jitters. To study the BPM resolution through the wire-based approach, the dedicated standalone test bench was improved by adding a piezo stack. Now a relative nanometric movement between the BPM and the stretched wire is possible while sensing the position. The actuator is mounted on the hexapod and drives the BPM on a single direction (vertical axis). To reduce the impact of environmental factors, tests were repeated several times and averaged. Fig. 15 shows the linear dependency between the nanometric piezo elongation (25 nm) versus the adjacent ports phase argument of the scattering parameters. The gradient of the slopes is the resolution potential in the nanometric regime.

5.4. Fiducialization

The measurements of the electrical center presented so far were all relative units or referenced to the hexapod position. To precisely locate the electrical center w.r.t. an external absolute target (fiducialization) and detect the electrical-to-geometrical offset, the test bench was moved to the metrology laboratory at CERN. Further measurements took place on a CMM, with a maximum permitted error (MPE) of $\pm(1.2\ \mu m + L/500\ mm)$, where L is the length of the device under test in mm. The wire is stretched through the BPM RF cavity. Its position is detected through a non-contact optical sensor. Three metallic spherical targets were placed on top of the BPM (see Fig. 16). The position of the spheres is sensed by the CMM non-contact sensors and their center of mass returns the position of the BPM.

The wire is fixed at both ends, its relative position with respect to the BPM is controlled by moving the hexapod in 4-DOF. Initially, the operator determines the wire axis, a point of origin O is fixed on this axis by the coordinate of one of the spherical targets. After each hexapod incremental step, we record the targets' coordinates acquired by the CMM and referenced to the initial origin of axis O. At the same time, the VNA acquires the scattering parameters. The geometrical center is measured through the interpolation of the flanges' perimeters. The coordinates of the electrical center in Fig. 16(a) are approximated by the projections of the centers of the two lateral flanges.

The plots in Fig. 17 show the electrical center w.r.t. the geometrical center of the BPM position cavity. Measurements of the phase argument between adjacent ports are projected onto the curve plotting the absolute position coordinates, which were detected by the CMM and referenced to the BPM geometrical center. The BPM is moved with the hexapod, the step sizes is 4 μm, both on the horizontal and vertical directions. The offset between the electrical and the mechanical centers of the BPM is returned by analyzing the phase arguments w.r.t. the CMM data.

The geometrical and electrical center coordinates are projected on the xy-plane at the section $Z = 0$ and summarized in Table 4, along with the electrical center coordinates and the horizontal and vertical offsets. A gap between the two centers is present as of manufacturing and brazing imperfections.

6. Summary and conclusions

We described innovative methods to fiducialize and characterize a resonant cavity BPM. These methods can easily be applied to other accelerator components or BPMs based on different technologies. The

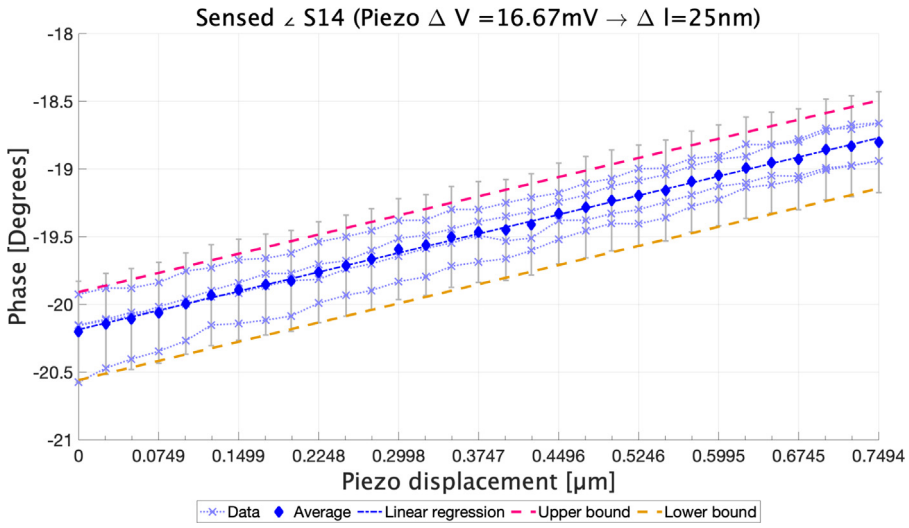

Fig. 15. S-parameter phase measurements for a linear scan with a step size of 25 nm.

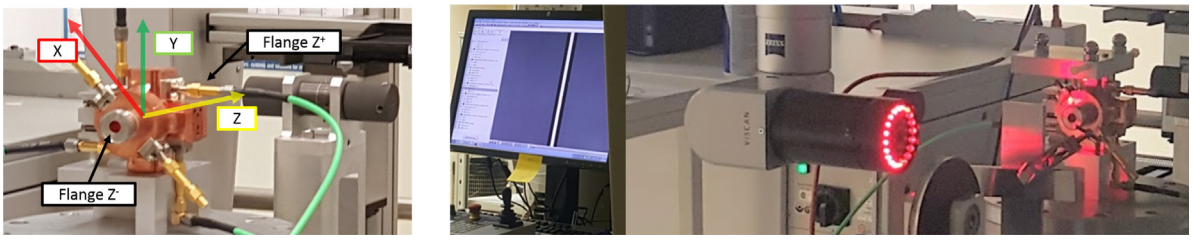

Fig. 16. Details of the measurement setup. (a) Spherical targets used for the BPM fiducialization, with coordinate system. (b) Optical sensor and image analysis acquisition of the wire stretched through the cavity BPM.

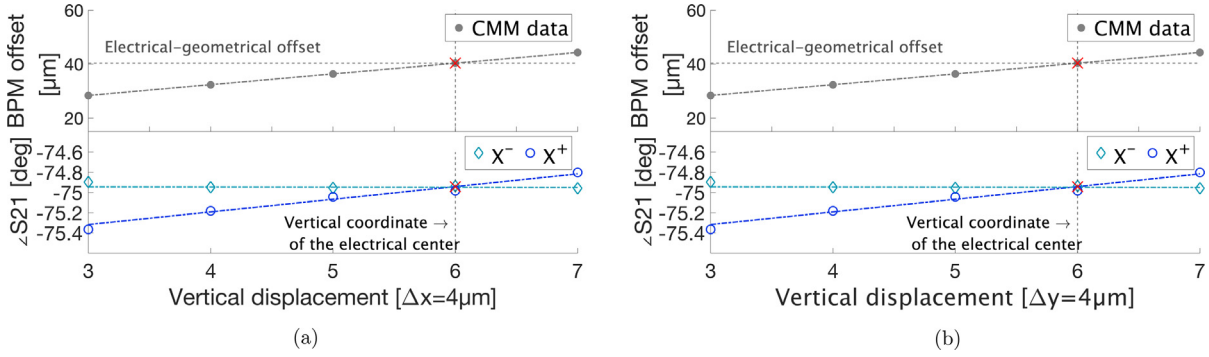

Fig. 17. Horizontal and vertical offsets between the electrical center and the geometrical center.

Table 4
Offset values in the detection of the electrical center.

Offset		
X [μm]	Y [μm]	Z [μm]
17.3	36.57	0

use of a dedicated stretched-wire test bench was the key element to demonstrate both the exact location of the electrical center of the cavity BPM and its nanometric resolution. Such achievements create new opportunities for the alignment of future colliders, in particular at the BPM-quadrupole interface. In fact, if the beam brightness is close to the diffraction limit, the commonly used alignment and stabilization techniques may not be sufficient. The accuracy of the scans combined with the presented fiducialization and alignment techniques allows the precise determination of the radial and linear offsets.

Declaration of competing interest

The authors declare that they have no known competing financial interests or personal relationships that could have appeared to influence the work reported in this paper.

Data availability

Data will be made available on request.

Acknowledgments

The research leading to these results has received funding from the European Union's 7th Framework Programme Marie Curie actions, grant agreement PITN-GA-2013- 606839.

References

[1] CDR CLIC, in: M. Aicheler, P. Burrows, M. Draper, T. Garvey, P. Lebrun, K. Peach, N. Phinney, H. Schmickler, D. Schulte, N. Toge (Eds.), A Multi-TeV Linear Collider Based on CLIC Technology: CLIC Conceptual Design Report, CERN-2012-007, 2012.

[2] Markus Aicheler, P.N. Burrows, N. Catalan, R. Corsini, M. Draper, J. Osborne, Daniel Schulte, Steinar Stapnes, M.J. Stuart, The compact linear collider (CLIC)-project implementation plan, 2019, arXiv preprint arXiv:1903.08655.

[3] D.A. Edwards, M.J. Syphers, An Introduction to the Physics of High Energy Accelerators, John Wiley & Sons, 2008.

[4] D. Schulte, Beam–beam effects in linear colliders, in: Proceedings of the CAS-CERN Accelerator School: Intensity Limitations in Particle Beams, Geneva, Switzerland, 2–11 November 2015, CERN Accelerator School (CAS), Geneva, Switzerland, 2015, pp. 431–445.

[5] O. Brunner, et al., The CLIC project, 2022.

[6] M. Wendt, Overview of recent trends and developments for BPM systems, in: 11th European Workshop on Beam Diagnostics and Instrumentation for Particle Accelerators (DIPAC2011), Hamburg, Germany, 16-18 May 2011, 2011, pp. 18–22.

[7] D. Caiazza, N. Catalan Lasheras, H. Mainaud Durand, M. Modena, C. Sanz, D. Tshilumba, V. Vlachakis, M. Wendt, S. Zorzetti, New solution for the high accuracy alignment of accelerator components, Phys. Rev. Accel. Beams 20 (8) (2017) 083501.

[8] Claude Sanz, Ahmed Cherif, Hélène Mainaud Durand, Paul Morantz, Paul Shore, Characterisation and measurement to the sub-micron scale of a reference wire position, in: 17th International Congress of Metrology, EDP Sciences, 2015, p. 13005.

[9] D. Caiazza, Metrological Performance Enhancement of Wire Methods for Magnetic Field Measurements in Particle Accelerators (Ph.D. thesis), Department of Engineering, University of Sannio, Benevento, 2017.

[10] N. Galindo Munoz, Development of Direct Measurement Techniques for the in-Situ Internal Alignment of Accelerating Structures (Ph.D. thesis), University of Valencia, Valencia, 2018.

[11] S. Zorzetti, Radio Frequency Characterization and Alignment to the Nanometer Scale of a Beam Position Monitor for Particle Accelerators (Ph.D. thesis), Universita di Pisa, Pisa, 2016.

[12] C. Sanz, Study on the Feasibility of a Non-Contact High Precision Sensor for Coordinate Measuring Machine (Ph.D. thesis), university of Cranfield, Cranfield, 2019.

[13] S. Kamugasa, Development and Validation of Frequency Scanning Interferometry Network for Compact LInear Collider Component Fiducialisation (Ph.D. thesis), ETH Zurich, Zürich, 2018.

[14] V. Vlachakis, Automated Micro-Triangulation for High Precision Fiducialisation and Alignment of Particle Accelerator Components (Ph.D. thesis), ETH Zurich, Zürich, 2021.

[15] A. Lunin, N. Solyak, M. Wendt, V. Yakovlev, Design of a submicron resolution cavity BPM for the CLIC main linac, TD-Note-TD-09 28 (2007).

[16] H. Schmickler, L. Søby, A. Lunin, N. Solyak, M. Wendt, Submicron multi-bunch BPM for CLIC, in: 1st International Particle Accelerator Conference (IPAC'10), Kyoto, Japan, 23-28 May 2010, JACOW, Geneva, Switzerland, 2010, pp. 1185–1187.

[17] N. Chritin, H. Schmickler, L. Søby, A. Lunin, N. Solyak, M. Wendt, V. Yakovlev, A high-resolution cavity BPM for the CLIC test facility, in: Beam Instrumentation Workshop (BIW2010), Santa Fe, New Mexico, USA, 2-6 May 2010, JACOW, Geneva, Switzerland, 2010, pp. 189–193.

[18] M. Gasior, R. Jones, T. Lefevre, H. Schmickler, K. Wittenburg, Introduction to beam instrumentation and diagnostics, 2016, arXiv preprint arXiv:1601.04907.

[19] S. Walston, S. Boogert, C. Chung, P. Fitsos, J. Frisch, J. Gronberg, H. Hayano, Y. Honda, Y. Kolomensky, A. Lyapin, et al., Performance of a high resolution cavity beam position monitor system, Nucl. Instrum. Methods Phys. Res. A 578 (1) (2007) 1–22.

[20] David H. Whittum, Yury Kolomensky, Analysis of an asymmetric resonant cavity as a beam monitor, Rev. Sci. Instrum. 70 (5) (1999) 2300–2313.

[21] Y.I. Kim, R. Ainsworth, A. Aryshev, S.T. Boogert, G. Boorman, J. Frisch, A. Heo, Y. Honda, W.H. Hwang, J.Y. Huang, et al., Cavity beam position monitor system for the Accelerator Test Facility 2, Phys. Rev. Spec. Top.-Accel. Beams 15 (4) (2012) 042801.

[22] L.C. Maier Jr., J.C. Slater, Field strength measurements in resonant cavities, J. Appl. Phys. 23 (1) (1952) 68–77.

[23] M. Nasserdine, S. Mengué, C. Bourcier, E. Richalot, Field measurements within a large resonant cavity based on the perturbation theory, Prog. Electromagn. Res. B 57 (2014) 1–20.

[24] Luke Aidan Dyks, Philip Burrows, P. Korysko, et al., Consolidation and Future Upgrades to the CLEAR User Facility at CERN, JACoW Publishing, Geneva, Switzerland, 2021.